high altitudes during the Tertiary in much of western North America (*24*). The contention that late Cenozoic uplift of mountain ranges and plateaus throughout the world was a trigger for the onset of the Ice Age (*5*) should be reevaluated.

REFERENCES AND NOTES

1. P. W. Richards, *The Tropical Rain Forest* (Cambridge Univ. Press, Cambridge, 1952); R. A. Spicer, *Trans. R. Soc. Edinburgh* **80**, 321 (1989); A. B. Herman and R. A. Spicer, *Nature* **381**, 330 (1996).
2. J. A. Wolfe and H. E. Schorn, *Paleobiology* **15**, 180 (1989).
3. D. I. Axelrod, *Univ. Calif. Publ. Geol. Sci.* **39**, 195 (1962); *ibid.* **34**, 91 (1958); *ibid.* **135**, 1 (1991); *ibid.* **137**, 1 (1992).
4. W. F. Ruddiman and J. E. Kutzbach, *J. Geophys. Res.* **94**, 409 (1989).
5. J. A. Wolfe, *Nature* **343**, 153 (1990); *U.S. Geol. Surv. Bull. 2040* (1993); *Annu. Rev. Earth Planet. Sci.* **23**, 119 (1995).
6. C. J. F. ter Braak, *Biometrics* **41**, 859 (1985); *Ecology* **67**, 1167 (1986); C. J. F. ter Braak and I. C. Prentice, *Adv. Ecol. Res.* **18**, 271 (1988).
7. The tabulations for the leaf assemblages were run with the software CANOCO. This software is available from Microcomputer Power, 111 Clover Lane, Ithaca, NY 14850.
8. H. J. B. Birks, S. M. Peglar, H. A. Austin, *An Annotated Bibliography of Canonical Correspondence Analysis and Related Constrained Ordination Methods 1986–1993* (Univ. of Bergen Botanical Institute, Bergen, Norway, 1994).
9. C. E. Forest, P. Molnar, K. A. Emanuel, *Nature* **374**, 347 (1995).
10. C. E. Forest, thesis, Massachusetts Institute of Technology (1996).
11. The database furnished earlier to Forest comprised 106 samples, including 25 that represent outliers and inliers in plots of samples on axes 1 and 2 (*5*). The elimination of these 25 samples reduced standard errors of estimates of environmental parameters and increased axis eigenvalues. Samples (including 12 from the largely deciduous vegetation of southern Sonora and Baja California) have subsequently been added to the database, which now comprises 97 samples, excluding the 25 outliers and inliers. Both the physiognomic and meteorological data sets, as well as the locality data for the new samples, can be obtained from J. A. Wolfe.
12. D. A. R. Povey, R. A. Spicer, P. C. England, *Rev. Palaeobot. Palynol.* **81**, 1 (1994).
13. B. J. Flower and J. P. Kennett, *Paleoceanography* **10**, 1095 (1995).
14. H. D. MacGinitie, *Carnegie Inst. Washington Publ.* **465**, 83 (1937).
15. E. E. Small and R. S. Anderson, *Science* **270**, 277 (1995).
16. J. A. Wolfe and H. E. Schorn, *Geol. Soc. Am. Abstr. Program* **26**, A521 (1994).
17. J. A. Wolfe, *U.S. Geol. Surv. Bull. 1964* (1992).
18. P. Molnar and W.-P. Chen, *J. Geophys. Res.* **88**, 1180 (1983); P. J. Coney and T. A. Harms, *Geology* **12**, 550 (1984).
19. P. Molnar and H. Lyon-Caen, *Geol. Soc. Am. Spec. Pap.* **218**, 179 (1988).
20. H. W. Meyer, *Palaeogeogr. Palaeoclimatol. Palaeoecol.* **99**, 71 (1992).
21. K. M. Gregory and C. G. Chase, *Geology* **20**, 581 (1992).
22. P. Molnar and P. C. England, *Nature* **346**, 29 (1990).
23. B. Wernicke *et al.*, *Science* **271**, 190 (1996).
24. R. A. Kerr, *ibid.* **275**, 1564 (1997).
25. Revisions to the taxonomy were made by Wolfe and Schorn before the analysis of some of these assemblages. Other than (*3, 14*), available sources include R. S. LaMotte, *Carnegie Inst. Washington Publ.* **455**, 57 (1936); C. Condit, *ibid.* **476**, 217 (1938); *ibid.* **553**, 57 (1944); D. I. Axelrod, *Univ. Calif. Publ. Geol. Sci.* **33**, 1 (1956); *ibid.* **129**, 1 (1985); J. A. Wolfe, *U. S. Geol. Surv. Prof. Pap. 454-N*, N1 (1964); and K. M. Renney, thesis, University of California, Davis (1969). In all instances, we examined original collections in the University of California Museum of Paleontology (Berkeley).
26. C. C. Swisher III, thesis, University of California, Berkeley (1992).

27. This work was partially supported by NSF (Atmospheric Sciences).

2 April 1997; accepted 28 April 1997

Photodissociation of $I_2^-(Ar)_n$ Clusters Studied with Anion Femtosecond Photoelectron Spectroscopy

B. Jefferys Greenblatt,* Martin T. Zanni,* Daniel M. Neumark†

Anion femtosecond photoelectron spectroscopy was used to follow the dynamics of the $I_2^-(Ar)_6$ and $I_2^-(Ar)_{20}$ clusters subsequent to photodissociation of the I_2^- chromophore. The experiments showed that photodissociation of the I_2^- moiety in $I_2^-(Ar)_6$ is complete by approximately 200 femtoseconds, just as in bare I_2^-, but also that attractive interactions between the departing anion fragment and the solvent atoms persisted for 1200 femtoseconds. Photodissociation of $I_2^-(Ar)_{20}$ results in caging of the I_2^- followed by recombination and vibrational relaxation on the excited $\tilde{A}\,^2\Pi_{g,3/2}$ and the ground $\tilde{X}\,^2\Sigma_u^+$ states; these processes are complete in 35 and 200 picoseconds, respectively.

Understanding of the potential energy surfaces governing the dynamics of elementary chemical reactions in the gas phase has grown significantly during the past 10 years, largely because of the development of new frequency- and time-resolved experimental techniques (*1, 2*) combined with theoretical advances in quantum chemistry (*3*) and reaction dynamics (*4*). A very appealing new direction in this field is to investigate, in a systematic way, the effects of solvation on reaction dynamics. Studies of chemical reactions occurring within size-selected clusters provides an elegant means of achieving this goal, because one can monitor the changes that occur as a function of cluster size and ultimately learn how the dynamics of an elementary unimolecular or bimolecular reaction evolve as a condensed-phase environment is approached (*5*). It is particularly useful to perform such experiments on ionic clusters, for which size selection is straightforward. We recently performed a time-resolved study of the photodissociation dynamics of the I_2^- anion, using a new technique—anion femtosecond photoelectron spectroscopy (FPES) (*6*). We now apply this method to follow the dynamics that result from photodissociation of the I_2^- chromophore in the clusters $I_2^-(Ar)_6$ and $I_2^-(Ar)_{20}$. These experiments yielded time-resolved measurements of the anion-solvent interactions subsequent to photodissociation and, in the case of $I_2^-(Ar)_{20}$, provided new insight into the caging and recombination dynamics of the I_2^- moiety.

Anion FPES is a pump-probe experiment using laser pulses of ~100 fs duration in which a pump pulse photodissociates an anion (or anion chromophore in a cluster) and a probe pulse ejects an electron from the dissociating species. By measurement of the resulting photoelectron (PE) spectrum at various delay times, the experiment yields "snapshots" of the dissociation dynamics and, in particular, probes how the local environment of the excess electron evolves with time. This highly multiplexed experiment yields information on the entire photoexcited wavepacket at each delay time without having to vary the wavelength of the probe pulse; this is in contrast to most pump-probe experiments in which only an absorption of the probe pulse is monitored. Although FPES has also been applied to neutrals (*7–9*), the anion experiment is inherently mass-selective, making it especially useful in studies of size-selected clusters.

Our work here builds on the experiments of Lineberger and co-workers (*10–12*), who performed one-photon photodissociation and time-resolved pump-and-probe experiments on size-selected $I_2^-(CO_2)_n$ and $I_2^-(Ar)_n$ cluster anions, and on the time-resolved studies of neutral $I_2(Ar)_n$ clusters by Zewail and co-workers (*13*). The one-photon cluster anion experiments yielded the asymptotic daughter ion distributions as a function of initial cluster size; in particular, the relative amounts of "caged" $I_2^-(Ar)_{m1<n}$ products in which the I and I^- photofragments are trapped by the

Department of Chemistry, University of California, Berkeley, CA 94720, and Chemical Sciences Division, Lawrence Berkeley National Laboratory, Berkeley, CA 94720, USA.

*These authors contributed equally to this work.
†To whom correspondence should be addressed. E-mail: dan@radon.cchem.berkeley.edu

solvent atoms and eventually recombine, versus "uncaged" $I^-(Ar)_{m2<n}$ products in which trapping does not occur. Only uncaged products were observed from the photodissociation of $I_2^-(Ar)_6$, with ArI^- as the dominant product, indicating that there are not enough solvent atoms to trap the recoiling photofragments. In contrast, the solvent shell is approximately complete for $I_2^-(Ar)_{20}$, so that only caged products are seen. Moreover, photodissociation of $I_2^-(Ar)_{20}$ results in two distinct recombination channels formed with approximately equal yield: bare I_2^- and $I_2^-(Ar)_n$ with $\langle n \rangle = 11$. The time-resolved experiments on $I_2^-(Ar)_{20}$ yielded a time constant of 127 ps for recovery of the I_2^- absorption (*12*); this represents the overall time scale for recombination and relaxation of the I_2^- product. Our experiment provides a more complete picture of the dynamics following excitation of $I_2^-(Ar)_6$ and $I_2^-(Ar)_{20}$ and, in particular, clarifies the origin of the two product channels seen for $I_2^-(Ar)_{20}$.

The FPES experiment is described in detail elsewhere (6). Briefly, a pulsed, mass-selected beam of cold cluster anions is intercepted by the pump-and-probe pulses at the focus of a "magnetic bottle" time-of-flight PE spectrometer. The two laser pulses are generated by a Ti:sapphire oscillator–regenerative amplifier system (Clark MXR) operating at a repetition rate of 500 Hz. The pump pulse at 780 nm and the probe pulse at 260 nm are 80 and 100 fs long, respectively. The high laser repetition rate combined with the high (>50%) collection efficiency of the magnetic bottle analyzer results in rapid data acquisition; each spectrum is typically obtained in 40 to 80 s for I_2^- and $I_2^-(Ar)_6$, and 10 to 15 min for $I_2^-(Ar)_{20}$. At the ion beam energy used in this work (1750 eV), the electron energy resolution of the spectrometer at 1 eV electron kinetic energy (eKE) is 0.25 eV for I_2^-, 0.18 eV for $I_2^-(Ar)_6$, and 0.12 eV for $I_2^-(Ar)_{20}$.

The relevant potential energy curves for I_2^- and I_2 are shown in Fig. 1 (*14–16*). The pump pulse excites the $\tilde{A}'\ ^2\Pi_{g,1/2} \leftarrow \tilde{X}\ ^2\Sigma_u^+$ transition in I_2^-, creating a localized wavepacket on the repulsive excited state. The probe pulse detaches the dissociating ion to the various low-lying states of I_2 (Fig. 1). In the bare ion, rapid and direct dissociation to $I^- + I(^2P_{3/2})$ occurs. However, when the same I_2^- transition is excited in an $I_2^-(Ar)_n$ cluster, the recoiling fragments interact with the Ar atoms, and the FPES experiment provides a sensitive probe of these interactions.

Figure 2 shows selected PE spectra at various pump-probe delay times τ for I_2^-, $I_2^-(Ar)_6$, and $I_2^-(Ar)_{20}$. The spectra of I_2^- in Fig. 2A have been discussed in detail previously (6). Two peaks centered at eKE = 1.70 eV and 0.75 eV rise monotonically with increasing delay; these correspond to photodetachment of the I^- photodissociation product to the $I(^2P_{3/2})$ and $I^*(^2P_{1/2})$ atomic states, respectively. In addition, there is a transient signal peaking at τ = 50 to 100 fs on the high electron energy side of each product peak attributed to the dissociating ions. The product peaks dominate the spectra by 200 fs, and no further changes are observed at later times, indicating dissociation is complete.

The $I_2^-(Ar)_6$ spectra in Fig. 2B resemble the I_2^- spectra at first glance, particularly for $\tau < 240$ fs. By τ = 240 fs, the spectra for $I_2^-(Ar)_6$ consist of two peaks clearly analogous to the atomic $I \leftarrow I^-$ transitions in the I_2^- spectra. However, these two "I^-" peaks occur at an eKE 0.12 eV lower than for bare I^-. In addition, the peaks gradually shift toward an eKE 0.10 eV higher than for bare I^- as τ increases from 240 to 1200 fs. The spectra do not change after τ = 1200 fs.

The spectra for $I_2^-(Ar)_{20}$ in Fig. 2C show the same general trends up to τ = 1 ps. Two new trends are seen at later times, however. First, as τ increases from 1 to 35 ps, the two "I^-" peaks apparently reverse direction and shift toward lower eKE by about 0.14 eV. Second, a new, broad feature at high electron energy (eKE > 1.6 eV) appears at $\tau > 4$ ps. This feature shifts toward lower eKE until τ = 200 ps, after which no further significant evolution occurs. Two small peaks between the two "I^-" peaks also grow in on this time scale.

The $I_2^-(Ar)_6$ spectra indicate that the dynamics subsequent to photoexcitation can be divided into two time regimes. At early times ($\tau \leq 240$ fs), the I_2^- chromophore dissociates to $I^- + I$. The similarity between these spectra and those for I_2^-

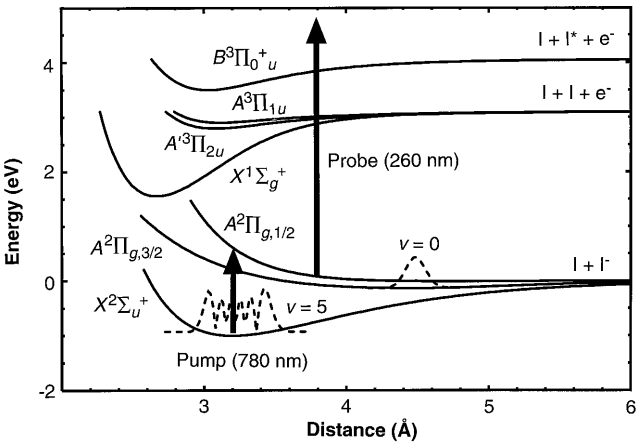

Fig. 1. Potential energy curves for the low-lying electronic states of I_2^- and I_2. The curves for the I_2^- $\tilde{X}\ ^2\Sigma_u^+$ and $\tilde{A}'\ ^2\Pi_{g,1/2}$ states are taken from (*15*) and (*14*), respectively. For the $\tilde{X}$ state, D_e = 1.014 eV, R_e = 3.205 Å, and the harmonic frequency ω_e = 110 cm^{-1}. The $\tilde{A}\ ^2\Pi_{g,3/2}$ state is described in the text. The v = 0 and v = 5 wave functions on the I_2^- $\tilde{X}$ and $\tilde{A}$ states are also shown (see text). The I_2 curves are from (*16*) and references therein.

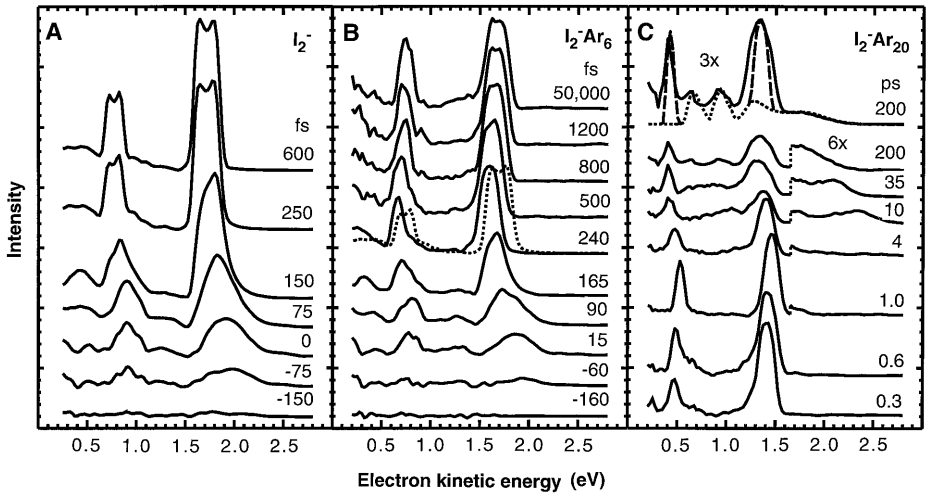

Fig. 2. Anion femtosecond photoelectron spectra at various pump-probe delay times τ for (**A**) I_2^-, (**B**) $I_2^-(Ar)_6$, and (**C**) $I_2^-(Ar)_{20}$. In (B), the I_2^- spectrum at 250 fs (· · ·) is superimposed on the $I_2^-(Ar)_6$ spectrum at 240 fs for comparison. In (C), the signal at eKE > 1.6 eV is magnified by a factor of 6 for $\tau \geq 1$ ps. A simulation of the $I_2^-(Ar)_{20}$ spectrum at 200 ps is superimposed on the experimental spectrum at the top of (C). Contributions to the simulation from transitions originated from the I_2^- $\tilde{X}$ state (· · ·) and $\tilde{A}$ state (---) are indicated.

indicates that the primary bond-breaking dynamics are not affected by clustering and that this process is complete by 240 fs. The interpretation of the spectra in the second time regime, from 240 to 1200 fs, is aided by our previous measurements of the electron affinities of $I(Ar)_n$ clusters, which show that each Ar atom increases the electron affinity by 25 meV (*17*). The 0.12 eV energy offset in the "I^-" peaks at 240 fs relative to bare I^- is what would be expected for an I^- ion bound to five Ar atoms. As τ increases, the shifts of these peaks toward higher eKE indicate that the I^- is interacting with progressively fewer Ar atoms. The spectrum at 1200 fs is that expected for ArI^-; this is consistent with the mass-resolved experiments (*11*) that show ArI^- to be the dominant product from $I_2^-(Ar)_6$ photodissociation. Thus, the evolution of the spectra from 240 to 1200 fs reflects the progressively weaker interactions between the solvent atoms and the I^- fragment, with formation of the asymptotic ArI^- product complete by 1200 fs.

One picture of the dynamics during the second time regime consistent with the spectra is that once the I_2^- chromophore is dissociated, the neutral I atom is ejected, leaving behind a vibrationally hot $I^-(Ar)_n$ cluster from which Ar atoms evaporate until the available energy is dissipated, with ArI^- as the stable product. This picture is suggested by molecular dynamics simulations carried out by Amar (*18*) on $Br_2^-(CO_2)_n$ clusters. However, recent molecular dynamics simulations by Faeder *et al.* (*19, 20*) suggest a somewhat different mechanism. Their calculations predict that the equilibrium geometry of $I_2^-(Ar)_6$ is an open, highly symmetric structure consisting of a ring of Ar atoms lying in the plane that bisects the I_2^- bond. When the I_2^- is dissociated, the I and I^- fragments separate sufficiently rapidly so that the Ar atoms do not cluster around the I^- fragment. Instead, the departing I^- fragment abstracts one of the solvent atoms, on average, as the cluster breaks up. The shifts in the PE spectrum during the second time regime are qualitatively consistent with this picture, in that as the I^- fragment leaves the cluster, its attractive interactions with the solvent atoms decrease and the electron affinity drops.

We next consider the $I_2^-(Ar)_{20}$ clusters, for which caging is complete (*11*). The overall appearance and evolution of these spectra from 300 fs to 1 ps is similar to that seen for $I_2^-(Ar)_6$, in that there are two "I^-" peaks that shift toward higher electron energy as τ increases. Thus, up to $\tau = 1$ ps, the cluster contains I and I^- fragments that are essentially independent of one another. The shifting of the peaks toward higher eKE can again be explained as a progressive weakening of the interactions between the I^- fragment and the solvent atoms. This is probably due to a combination of evaporation of solvent atoms induced by the recoil energy of the I and I^- fragments (~0.6 eV) and the rather large excursions that the I^- fragment makes within the cluster as the I and I^- photoproducts separate on the repulsive $\tilde{A}'\ ^2\Pi_{g,1/2}$ state. Molecular dynamics simulations by Batista and Coker (*21*) predict the interiodine separation increases to 8 to 10 Å after 1 ps has elapsed, a distance comparable to the original size of the cluster, and it is likely that the strength of the solvent interactions with the I^- decreases while this occurs.

The evolution of the $I_2^-(Ar)_{20}$ spectra at later times can be explained as a result of recombination of the I and I^- on the two lowest potential energy curves in Fig. 1. The shifting of the two "I^-" peaks toward lower energy from $\tau = 1$ to 35 ps is consistent with recombination and vibrational relaxation on the $\tilde{A}\ ^2\Pi_{g,3/2}$ curve. Recent ab initio calculations predict that the equilibrium bond length $R_e = 4.18$ Å and the well depth $D_e = 0.11$ eV for this state (*22*). Figure 1 shows that at such a large internuclear distance, photodetachment will access the neutral potential energy curves near their asymptotic energies. This will yield two peaks approximately separated by the I atom spin-orbit splitting, but shifted toward lower electron energy compared to bare I^- by the well depth (D_e) of the $\tilde{A}\ ^2\Pi_{g,3/2}$ state and the sum of the attractive interactions with the remaining Ar atoms. If we use an approximate binding energy of 73 meV per Ar atom (*11*), the total energy released by the recoiling photofragments and by vibrational relaxation of the I_2^- to the $v = 0$ level of the ab initio $\tilde{A}\ ^2\Pi_{g,3/2}$ state is sufficient to evaporate nine Ar atoms, so this excited state recombination mechanism is the likely origin of the $I_2^-(Ar)_{\langle n\rangle = 11}$ product seen by Lineberger and co-workers (*11*). From these considerations, it is reasonable to attribute the signal at eKE > 1.6 eV to recombination on the $\tilde{X}\ ^2\Sigma_u^+$ state followed by vibrational relaxation. This can release enough energy to evaporate all of the Ar atoms, leaving $I_2^-(v = 8)$ in the limit of zero photofragment KE.

In order to test these assignments, we simulated the spectrum at 200 ps, assuming photodetachment to occur from $I_2^-(Ar)_{11}$ with the I_2^- chromophore in the $v = 0$ level of the $\tilde{A}\ ^2\Pi_{g,3/2}$ state, and from I_2^- ($\tilde{X}\ ^2\Sigma_u^+$) in a mixture of vibrational levels. The simulations involve calculating the Franck-Condon factors between the anion and neutral vibrational wave functions and scaling the results for different electronic transitions to best match the experimental intensities. For the $\tilde{A}\ ^2\Pi_{g,3/2}$ state, R_e and D_e were taken to be 4.5 Å and 0.16 eV, respectively, with both values differing somewhat from the ab initio values; these differences may reflect, in part, the influence of the remaining Ar atoms in the cluster. Best results for the $\tilde{X}\ ^2\Sigma_u^+$ state were obtained using a vibrational distribution with $\langle v\rangle = 5$. The results reproduce the experimental spectrum quite well (Fig. 2C). The I_2^- ($\tilde{A}\ ^2\Pi_{g,3/2}$, $v = 0$) and I_2^- ($\tilde{X}\ ^2\Sigma_u^+$, $v = 5$) vibrational wave functions are superimposed on the appropriate potential energy curves in Fig. 1. Note that photodetachment from the inner turning point of the I_2^- ($\tilde{X}\ ^2\Sigma_u^+$, $v = 5$) wave function is responsible for the signal at eKE > 1.6 eV; the outer turning point contributes to the "I^-" peak at 1.35 eV along with photodetachment from the I_2^- $\tilde{A}\ ^2\Pi_{g,3/2}$ state.

The shifting of the signal at eKE > 1.6 eV toward lower energy from 10 to 200 ps results from vibrational relaxation of the ground state I_2^- accompanied by evaporative cooling of the Ar atoms in a series of reactions of the type $I_2^-(v'')(Ar)_n \rightarrow I_2^-(v' < v'')(Ar)_{n-1} + Ar$. As the I_2^- vibrational quantum number decreases, the contribution to the PE spectrum from the inner turning point of the vibrational wave function shifts toward lower eKE. Although this is partially compensated by reduction of the electron affinity as Ar atoms evaporate, our simulations of the PE spectra showed a net shift of the signal in this region toward lower eKE as the cluster cools. By comparing these simulations with the experimental spectra and starting with the I_2^- vibrational distribution at 200 ps, the average number of Ar atoms $\langle n\rangle$ and I_2^- vibrational quantum number $\langle v\rangle$ for $\tau < 200$ ps can be estimated. We find that $\langle n\rangle = 2$ and $\langle v\rangle = 17$ at $\tau = 35$ ps, and $\langle n\rangle = 4.5$ and $\langle v\rangle = 32$ at $\tau = 10$ ps. Therefore, it appears that 15 or 16 of the original 20 solvent atoms evaporate in the first 10 ps and that the evaporation rate slows down markedly at later times.

Our spectra yielded the following picture of the dynamics resulting from photoexcitation of $I_2^-(Ar)_{20}$. As with I_2^- and $I_2^-(Ar)_6$, dissociation of the I_2^- chromophore is complete by 300 fs. Between 300 fs and 1 ps, the interaction between the I and I^- atoms within the cluster is very weak. After 1 ps, the I and I^- atoms recombine on either of the two lower-lying attractive potential energy surfaces. Recombination on the $\tilde{A}\ ^2\Pi_{g,3/2}$ state leads to $I_2^-(Ar)_{\langle n\rangle = 11}$ product in which the I_2^- is vibrationally cold, whereas recombination on the $\tilde{X}\ ^2\Sigma_u^+$ state results in bare I_2^- with $\langle v\rangle = 5$. The first process is complete by 35 ps, whereas the second, involving considerably more energy flow between the I_2^- and the solvent atoms, is finished after 200 ps. Although recombination on the $\tilde{A}\ ^2\Pi_{g,3/2}$

state was proposed as a possible mechanism in Lineberger's earlier study (*11*), our experiments provide conclusive spectroscopic evidence that this occurs.

REFERENCES AND NOTES

1. A. H. Zewail, *J. Phys. Chem.* **100**, 12701 (1996).
2. P. L. Houston, *ibid*., p. 12757.
3. M. H. Head-Gordon, *ibid*., p. 13213.
4. G. C. Schatz, *ibid*., p. 12839.
5. A. W. Castleman and K. H. Bowen, *ibid*., p. 12911.
6. B. J. Greenblatt, M. T. Zanni, D. M. Neumark, *Chem. Phys. Lett.* **258**, 523 (1996).
7. D. R. Cyr and C. C. Hayden, *J. Chem. Phys.* **104**, 771 (1996).
8. P. Ludowise, M. Blackwell, Y. Chen, *Chem. Phys. Lett.* **258**, 530 (1996).
9. A. Assion, M. Geisler, J. Helbing, V. Seyfried, T. Baumert, *Phys. Rev. A* **54**, R4605 (1996).
10. J. M. Papanikolas *et al*., *J. Chem. Phys.* **99**, 8733 (1993).
11. V. Vorsa, P. J. Campagnola, S. Nandi, M. Larsson, W. C. Lineberger, *ibid.* **105**, 2298 (1996).
12. V. Vorsa, S. Nandi, P. J. Campagnola, M. Larsson, W. C. Lineberger, *ibid.* **106**, 1402 (1997).
13. Q. Liu, J.-K. Wang, A. H. Zewail, *Nature* **364**, 427 (1993).
14. E. C. M. Chen and W. E. Wentworth, *J. Phys. Chem.* **89**, 4099 (1985).
15. M. T. Zanni, T. Taylor, B. J. Greenblatt, B. Soep, D. M. Neumark, in preparation.
16. D. R. T. Appadoo *et al*., *J. Chem. Phys.* **104**, 903 (1996).
17. I. Yourshaw, Y. X. Zhao, D. M. Neumark, *ibid.* **105**, 351 (1996).
18. L. Perera and F. G. Amar, *ibid.* **90**, 7354 (1989).
19. J. Faeder, N. Delaney, P. E. Maslen, R. Parson, *Chem. Phys. Lett.* **270**, 196 (1997).
20. J. Faeder and R. Parson, in preparation.
21. V. S. Batista and D. F. Coker, *J. Chem. Phys*. **106**, 7102 (1997).
22. P. E. Maslen, J. Faeder, R. Parson, *Chem. Phys. Lett.* **263**, 63 (1997).

23. Supported by NSF under grant number CHE-9404735 and the Defense University Research Instrumentation Program under grant number F49620-95-1-0078. We thank J. Faeder, P. Maslen, V. Batista, and R. Parson for helpful discussions and for providing access to unpublished results. We are grateful to R. J. Le Roy for a copy of *RKR1: A Computer Program for Implementing the First-Order RKR Method for Determining Diatom Potential Energy Curves from Spectroscopic Constants*.

19 February 1997; accepted 12 May 1997

Infrared Spectrum of a Molecular Ice Cube: The S_4 and D_{2d} Water Octamers in Benzene-$(Water)_8$

Christopher J. Gruenloh, Joel R. Carney, Caleb A. Arrington, Timothy S. Zwier,* Sharon Y. Fredericks, Kenneth D. Jordan*

Resonant two-photon ionization, ultraviolet hole-burning, and resonant ion-dip infrared (RIDIR) spectroscopy were used to assign and characterize the hydrogen-bonding topology of two conformers of the benzene-$(water)_8$ cluster. In both clusters, the eight water molecules form a hydrogen-bonded cube to which benzene is surface-attached. Comparison of the RIDIR spectra with density functional theory calculations is used to assign the two $(water)_8$ structures in benzene-$(water)_8$ as cubic octamers of D_{2d} and S_4 symmetry, which differ in the configuration of the hydrogen bonds within the cube. OH stretch vibrational fundamentals near 3550 wave numbers provide unique spectral signatures for these "molecular ice cubes."

The gas-phase water octamer (W_8) holds a unique position among water clusters. From a structural viewpoint, both ab initio (*1, 2*) and model-potential (*1, 3–5*) calculations have predicted that the lowest energy structure for the octamer is nominally cubic, with the eight tricoordinated water molecules taking up positions at the corners of the cube. Such H-bond–deficient water molecules are known to be present at the surface of ice (*6*) and liquid water (*7*), and the cubic W_8 cluster enables the study of tricoordinate water molecules free from interference from the tetracoordinated molecules that dominate the bulk condensed phases. Furthermore, the cubic water clusters are prototypical building blocks for larger fused-cubic or cuboid structures, which have been proposed to play an important role in larger $(water)_n$ clusters (*4, 5*).

C. J. Gruenloh, J. R. Carney, C. A. Arrington, T. S. Zwier, Department of Chemistry, Purdue University, West Lafayette, IN 47907–1393, USA.

S. Y. Fredericks and K. D. Jordan, Department of Chemistry, University of Pittsburgh, Pittsburgh, PA 15260, USA.

*To whom correspondence should be addressed. E-mail: zwier@chem.purdue.edu, jordan@cpwsca.psc.edu

The water octamer can form six cubic structures, which differ in the orientations of the H bonds in the cube. Of these, the D_{2d} and S_4 symmetry structures have been calculated to be ~2 kcal/mol more strongly bound than the other four (*4*). The D_{2d} and S_4 structures each contain 12 H bonds: four in each of two cyclic tetramer subunits, and four bridging the two tetramers. The two structures are distinguished in having the H bonds within the tetramers oriented in the opposite (D_{2d}) or same (S_4) directions.

One of the most powerful spectroscopic probes of H-bonding networks is the OH stretch region of the infrared (IR) (*8*). The vibrational frequency and IR intensity of the OH stretch fundamentals are sensitive functions of the number, type, and strength of H bonds in which each OH group participates. Recent IR spectroscopic studies of small water (W_n) (*9*) and benzene-$(water)_n$ (BW_n) clusters (*10–13*) have provided insight into the structural and dynamic consequences of networks of H bonds. Here we report the corresponding OH-stretch IR spectral signatures for the D_{2d} and S_4 water octamers complexed to a single benzene molecule. The benzene molecule provides a means for both size and conformational selection of the clusters and weakly perturbs the W_8 cluster so that intensity is induced in many of the IR transitions that would otherwise be symmetry forbidden.

Ultraviolet spectra of the BW_n clusters were recorded with the use of resonant two-photon ionization (R2PI)–time-of-flight mass spectroscopy (*13–15*), monitoring the BW_6^+ and BW_7^+ mass channels (Fig. 1, curves A and B, respectively) in the origin region of the $S_1 \leftarrow S_0$ transition from the ground to the first excited singlet state of benzene. This transition from the lowest vibrational level of the S_0 state to the lowest vibrational level of the S_1 state is electric-dipole forbidden (*16*); however, in the BW_8 clusters, the presence of the water molecules lowers the symmetry, thereby inducing some intensity in the transition.

The assignment of a spectral transition to a given neutral cluster size must take into account the fragmentation of the cluster that can follow photo-ionization. Previous work (*13, 14*) has shown that in one-color R2PI experiments, BW_n clusters with $n = 1$ to 6 fragment after photo-ionization by loss of a single water molecule ($BW_n + 2h\nu \rightarrow BW_{n-1}^+ + W$), but larger clusters fragment to give both BW_{n-1}^+ and BW_{n-2}^+ (*14*). Thus, most of the structure in the BW_6^+ mass channel (Fig. 1, curve A) is from BW_7 and BW_8, whereas that in the BW_7^+ channel (Fig. 1, curve B) arises from BW_8 and BW_9. The set of four transitions marked in Fig. 1 appears primarily in the BW_7^+ mass channel but also in BW_6^+ and is therefore assigned to the BW_8 neutral cluster.

To determine whether more than one species contributes to the set of ultraviolet (UV) transitions assigned to BW_8, UV-UV hole-burning spectroscopy was performed (*17*). In these spectra, a high-power UV laser pulse was used to remove a significant fraction of the ground-state population of a given species. A second UV laser was then tuned through the spectrum while the difference in ion signal with and without the hole-burning laser present was recorded.